Multi-Polarization SAR Change Detection: Unstructured Versus Structured GLRT

Vincenzo Carotenuto*, Carmine Clemente†, Antonio De Maio*,
John Soraghan† and Salvatore Iommelli*
*Università degli Studi di Napoli "Federico II", DIETI, via Claudio 21, I-80125 Napoli, Italy
E-mail: vincenzo.carotenuto@unina.it, ademaio@unina.it, s.iommelli@unina.it
†University of Strathclyde, CESIP, EEE, 204, George Street, G1 1XW, Glasgow, UK
E-mail: carmine.clemente@strath.ac.uk, j.soraghan@strath.ac.uk

***Abstract*—The problem of coherent multi-polarization SAR change detection exploiting data collected from N multiple polarimetric channels, is addressed in this paper. The change detection problem is formulated as a binary hypothesis testing problem and a special block-diagonal structure for the polarimetric covariance matrix is forced to design a novel detector based on the Generalized Likelihood Ratio Test criterion. It is shown that the new decision rule ensures the Constant False Alarm Rate (CFAR) property. At the analysis stage, results on both simulated and real high resolution SAR data show the effectiveness of the proposed decision rule and its superiority against the traditional unstructured GLRT in some scenarios of practical interest.**

I. Introduction

Among all the civilian and defence applications of Synthetic Aperture Radar (SAR) images, change detection is one of the most challenging. Starting from a pair of co-registered temporally spaced SAR images representing an area of interest, change detection represents the capability to identify changes occurred during the time between the two acquisitions [1], [2]. When the change detection is performed exploiting only the intensity information of the image pair the technique is named incoherent change detection whereas if both amplitude and phase of the reference and test images are exploited the technique assume the name of coherent change detection. In [3], [4], the multi-polarization signal model for the SAR change detection problem is laid down, the detection problem is formulated as a binary hypothesis test, and a decision rule based on the Generalized Likelihood Ratio Test (GLRT) is developed. Moreover, a performance analysis [3] of the GLRT is given in the form of Receiver Operating Characteristics (ROC), namely detection Probability (P_d) versus false alarm Probability (P_{fa}), quantifying the benefits of the multi-polarization information in SAR change detection. In [5] a new and systematic framework for change detection based on the theory of invariance in hypothesis testing problems was developed for the multi-polarimetric coherent change detection problem.

In this paper we exploit the block-diagonal structure for the polarimetric covariance matrix introduced in [6] and devise a new decision rule based on the GLRT criterion. Remarkably, it ensures the CFAR property with respect to the unknown polarimetric covariance provided that it complies with a certain design structure. At the analysis stage we assess the performance of the new structured GLRT also in comparison with the benchmark clairvoyant optimum detector and the GLRT derived in [3] without the exploitation of the special covariance structure forced by polarization diversity. The analysis, conducted both on simulated as well as on real high resolution SAR data, shows the effectiveness of the structured GLRT and its superiority over the classic unstructured GLRT is some scenarios of practical interest.

The remainder of the paper is organized as follows. In Section II, the multi-polarization SAR change detection problem is formulated and the GLRT proposed in [3] is reported. In Section III the derivation of the novel structured GLRT is introduced while, in Section IV, the performance of the new detector is assessed for both simulated and real multi-polarization SAR images. Finally, in Section V, conclusions are provided.

A. Notation

We adopt the notation of using boldface for vectors and matrices. The conjugate transpose operator is denoted by the symbol $(\cdot)^\dagger$ while $\mathrm{tr}\,(\cdot)$ and $\det(\cdot)$ are respectively the trace and the determinant of the square matrix argument. Finally, $\mathbf{0}$ denotes the matrix with zero entries (its size is determined from the context), while $\mathcal{H}_N^{++}$ denotes, the set of $N \times N$ Hermitian positive definite matrices.

II. Problem Formulation

A multi-polarization SAR sensor measures for each pixel of the image under test $N = 3$ complex returns, collected from different polarimetric channels (HH, VV, and HV). The N returns from the same pixel are stacked in the specific order HH, VV, and HV (to form the vector $\boldsymbol{X}(l, m)$, where $l = 1, \dots, L$ and $m = 1, \dots, M$ (L and M represent the vertical and horizontal size of the image, respectively). Therefore, the sensor provides a 3-D data stack $\boldsymbol{X}$ of size $M \times L \times N$ which is referred to in the following as a datacube and is illustrated in Figure 1.

For SAR change detection applications, we assume that two datacubes $\boldsymbol{X}$ (reference data) and $\boldsymbol{Y}$ (test data) of the same geographic area are available. Furthermore we assume

978-1-4799-5294-6/14/$31.00 ©2014 IEEE

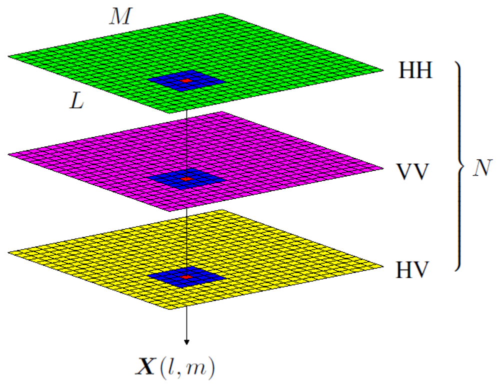

Fig. 1: Construction of the datacube.

that they are collected from two different sensor passes and are accurately pixel aligned (co-registrated). We focus on the problem of detecting the presence of possible changes in a rectangular neighbourhood $\mathcal{A}$, with size $K = W_1 \times W_2 \geq N$, of a given pixel. To this end, we denote by $\boldsymbol{R}_X$ ($\boldsymbol{R}_Y$) the matrix whose columns are the vectors of the polarimetric returns from the pixels of $\boldsymbol{X}$ ($\boldsymbol{Y}$) which fall in the region $\mathcal{A}$ and $\boldsymbol{S}_X = \boldsymbol{R}_X \boldsymbol{R}_X^\dagger$ ($\boldsymbol{S}_Y = \boldsymbol{R}_Y \boldsymbol{R}_Y^\dagger$).

The matrices $\boldsymbol{R}_X$ and $\boldsymbol{R}_Y$ are modelled as statistically independent random matrices. Moreover, the columns of $\boldsymbol{R}_X$ ($\boldsymbol{R}_Y$) are assumed statistically independent and identically distributed random vectors drawn from a complex circular zero-mean Gaussian distribution with positive definite covariance matrix $\boldsymbol{\Sigma}_X$ ($\boldsymbol{\Sigma}_Y$), complying with the structure introduced in [6], i.e.

$$\boldsymbol{\Sigma}_X \in \Xi \qquad (\boldsymbol{\Sigma}_Y \in \Xi),$$

where

$$\Xi = \left\{ \boldsymbol{\Sigma} \in \mathcal{H}_N^{++} \,:\, \boldsymbol{\Sigma} = \begin{pmatrix} \boldsymbol{\Sigma}_1 & \boldsymbol{0} \\ \boldsymbol{0} & \sigma^2 \end{pmatrix} \right\}, \tag{1}$$

Under the aforementioned settings, the change detection problem in the region $\mathcal{A}$ can be formulated in terms of the following binary hypothesis test

$$\begin{cases} H_0 : \boldsymbol{\Sigma}_X = \boldsymbol{\Sigma}_Y \\ H_1 : \boldsymbol{\Sigma}_X \neq \boldsymbol{\Sigma}_Y \end{cases} \tag{2}$$

where the null hypothesis H_0 of change absence is tested versus the alternative H_1. Exploiting the Gaussian assumption together with the covariance structure (1), we can write the joint probability density function (pdf) of $\boldsymbol{R}_X$ and $\boldsymbol{R}_Y$ as

$$\begin{aligned} & f_{\boldsymbol{R}_X,\boldsymbol{R}_Y}(\boldsymbol{R}_X, \boldsymbol{R}_Y | H_1, \boldsymbol{\Sigma}_{X,1}\boldsymbol{\Sigma}_{Y,1}, \sigma^2_{X,1}, \sigma^2_{Y,1}) = \\ & \frac{1}{\pi^{6K} \det^K(\boldsymbol{\Sigma}_{X,1}) \det^K(\boldsymbol{\Sigma}_{Y,1}) \sigma^{2K}_{X,1}\sigma^{2K}_{Y,1}} \\ & \exp\left\{ -\mathrm{tr}\left[\boldsymbol{\Sigma}_{X,1}^{-1}\boldsymbol{S}_{X,1} + \boldsymbol{\Sigma}_{Y,1}^{-1}\boldsymbol{S}_{Y,1} + \frac{\widehat{\sigma^2}_{X,1}}{\sigma^2_{X,1}} + \frac{\widehat{\sigma^2}_{Y,1}}{\sigma^2_{Y,1}} \right] \right\}, \end{aligned} \tag{3}$$

and

$$\begin{aligned} & f_{\boldsymbol{R}_X,\boldsymbol{R}_Y}(\boldsymbol{R}_X, \boldsymbol{R}_Y | H_0, \boldsymbol{\Sigma}_{X,1}, \sigma^2_{X,1}) = \\ & \frac{1}{\pi^{6K} \det^{2K}(\boldsymbol{\Sigma}_{X,1}) \sigma^{4K}_{X,1}} \\ & \exp\left\{ -\mathrm{tr}\left[\boldsymbol{\Sigma}_{X,1}^{-1}(\boldsymbol{S}_{X,1} + \boldsymbol{S}_{Y,1}) + \frac{\widehat{\sigma^2}_{X,1} + \widehat{\sigma^2}_{Y,1}}{\sigma^2_{X,1}} \right] \right\}, \end{aligned} \tag{4}$$

where $\boldsymbol{S}_X$ and $\boldsymbol{S}_Y$ are partitioned as

$$\boldsymbol{S}_X = \begin{bmatrix} \boldsymbol{S}_{X,1} & \boldsymbol{S}_{X,2} \\ \boldsymbol{S}_{X,2}^\dagger & \widehat{\sigma^2}_{X,1} \end{bmatrix} \qquad \boldsymbol{S}_Y = \begin{bmatrix} \boldsymbol{S}_{Y,1} & \boldsymbol{S}_{Y,2} \\ \boldsymbol{S}_{Y,2}^\dagger & \widehat{\sigma^2}_{Y,1} \end{bmatrix}, \tag{5}$$

and $\widehat{\sigma^2}_{X,1}$ and $\widehat{\sigma^2}_{Y,1}$ are scalars.

In [3], the GLRT has been devised without considering the special structure (1) for $\boldsymbol{\Sigma}_X$ and $\boldsymbol{\Sigma}_Y$. The resulting detector, referred to in the following as unstructured GLRT, is

$$\frac{\det^2(\boldsymbol{S}_X + \boldsymbol{S}_Y)}{\det(\boldsymbol{S}_X)\det(\boldsymbol{S}_Y)} \underset{H_0}{\overset{H_1}{\gtrless}} T_U\,, \tag{6}$$

where T_U is the detection threshold set to ensure a given P_{fa} level. In the next section, we exploit the special covariance structure (1) induced by polarization diversity and derive the structured GLRT.

III. Structured GLRT Design

This approach is equivalent to replacing the unknown parameters in the likelihood ratio with their maximum likelihood estimates, under each hypothesis [7]. Specifically, the structured GLRT is the decision rule (7), and after substituting the pdfs defined in (3) and (4), we get (8).

Hence, performing the maximizations over the parameters we can recast (8) in the equivalent form

$$\frac{\det^{2K}(\boldsymbol{S}_{X,1} + \boldsymbol{S}_{Y,1})}{\det^K(\boldsymbol{S}_{X,1})\det^K(\boldsymbol{S}_{Y,1})} \frac{\left(\widehat{\sigma^2}_{X,1} + \widehat{\sigma^2}_{Y,1}\right)^{2K}}{\left(\widehat{\sigma^2}_{X,1}\widehat{\sigma^2}_{Y,1}\right)^K} \underset{H_0}{\overset{H_1}{\gtrless}} T_{S,1}\,, \tag{9}$$

with $T_{S,1}$ a modified version of $T_{S,0}$. Finally, after a monotonic transformation, we get the following equivalent form of the GLRT

$$\frac{\det^2(\boldsymbol{S}_{X,1} + \boldsymbol{S}_{Y,1})}{\det(\boldsymbol{S}_{X,1})\det(\boldsymbol{S}_{Y,1})} \frac{\left(\widehat{\sigma^2}_{X,1} + \widehat{\sigma^2}_{Y,1}\right)^2}{\widehat{\sigma^2}_{X,1}\widehat{\sigma^2}_{Y,1}} \underset{H_0}{\overset{H_1}{\gtrless}} T_S\,, \tag{10}$$

with T_S the modified detection threshold. It can be proved that (10), ensures the CFAR property with respect to both $\boldsymbol{\Sigma}_{X,1}$ and $\sigma^2_{X,1}$. Otherwise stated, the detection threshold ensuring a given False Alarm Rate (FAR) can be set independent of the two aforementioned parameters.

$$\frac{\max\limits_{\mathbf{\Sigma}_{X,1},\mathbf{\Sigma}_{Y,1},\sigma^2_{X,1},\sigma^2_{Y,1}} f_{\boldsymbol{R}_X,\boldsymbol{R}_Y}(\boldsymbol{R}_X,\boldsymbol{R}_Y|H_1,\mathbf{\Sigma}_{X,1}\mathbf{\Sigma}_{Y,1},\sigma^2_{X,1},\sigma^2_{Y,1})}{\max\limits_{\mathbf{\Sigma}_{X,1},\sigma^2_{X,1}} f_{\boldsymbol{R}_X,\boldsymbol{R}_Y}(\boldsymbol{R}_X,\boldsymbol{R}_Y|H_0,\mathbf{\Sigma}_{X,1},\sigma^2_{X,1})} \underset{H_0}{\overset{H_1}{\gtrless}} T_{S,0}\,. \tag{7}$$

$$\frac{\max\limits_{\mathbf{\Sigma}_{X,1},\mathbf{\Sigma}_{Y,1},\sigma^2_{X,1},\sigma^2_{Y,1}} \left\{ \frac{\exp\left[-\mathrm{tr}\left(\mathbf{\Sigma}^{-1}_{X,1}\boldsymbol{S}_{X,1}+\mathbf{\Sigma}^{-1}_{Y,1}\boldsymbol{S}_{Y,1}+\frac{\widehat{\sigma^2}_{X,1}}{\sigma^2_{X,1}}+\frac{\widehat{\sigma^2}_{Y,1}}{\sigma^2_{Y,1}}\right)\right]}{\pi^{6K}\det^K(\mathbf{\Sigma}_{X,1})\det^K(\mathbf{\Sigma}_{Y,1})\sigma^{2K}_{X,1}\sigma^{2K}_{Y,1}} \right\}}{\max\limits_{\mathbf{\Sigma}_{X,1},\sigma^2_{X,1}} \left\{ \frac{\exp\left[-\mathrm{tr}\left(\mathbf{\Sigma}^{-1}_{X,1}(\boldsymbol{S}_{X,1}+\boldsymbol{S}_{Y,1})+\frac{\widehat{\sigma^2}_{X,1}\widehat{\sigma^2}_{Y,1}}{\sigma^2_{X,1}}\right)\right]}{\pi^{6K}\det^{2K}(\mathbf{\Sigma}_{X,1})\sigma^{4K}_{X,1}} \right\}} \underset{H_0}{\overset{H_1}{\gtrless}} T_{S,0}\,. \tag{8}$$

IV. Performance Analysis

This section presents the performance analysis for the proposed scale invariant decision rules for both simulated and real data.

A. Performance Analysis on Simulated Data

This sub-section presents the performance analysis via computer simulated data of the detectors introduced in Sections II and III. In particular, the standard ROCs are computed for the unstructured and structured GLRTs and compared with the benchmark performance of the optimum Neyman-Pearson detector. In order to set the detection threshold, Monte Carlo simulations are used assuming $100/P_{fa}$ independent runs. Additionally, 10^5 independent trials are exploited to estimate P_d. As in [3] the theoretical covariance matrices considered to estimate the P_d are:

$$\mathbf{\Sigma}_X = \begin{pmatrix} 1 & 0.5 & 0 \\ 0.5 & 1 & 0 \\ 0 & 0 & 0.2 \end{pmatrix} \qquad \mathbf{\Sigma}_Y = 2\mathbf{\Sigma}_X,$$

while $\mathbf{\Sigma}_Y = \mathbf{\Sigma}_X$ was considered to estimate the P_{fa}.

The optimum receiver assumes that the actual covariance matrices are known, and can be expressed as:

$$\mathrm{tr}\left[\left(\mathbf{\Sigma}^{-1}_X-\mathbf{\Sigma}^{-1}_Y\right)\boldsymbol{S}_Y\right] \underset{H_0}{\overset{H_1}{\gtrless}} T, \tag{11}$$

which resorting to the special structure of $\mathbf{\Sigma}_X$ and $\mathbf{\Sigma}_Y$ leads to

$$\mathrm{tr}\left[\left(\mathbf{\Sigma}^{-1}_{X,1}-\mathbf{\Sigma}^{-1}_{Y,1}\right)\boldsymbol{S}_{Y,1}+\left(\frac{1}{\sigma^2_{X,1}}+\frac{1}{\sigma^2_{X,2}}\right)\hat{\sigma}^2_{Y,1}\right] \underset{H_0}{\overset{H_1}{\gtrless}} T. \tag{12}$$

The obtained ROCs for the cases of $W = 3, 5$ and 7 are shown in Figures 2, 3 and 4 respectively. In all cases the structured GLRT outperforms the unstructured one, while the optimum receiver provides the benchmark performance. For example for the case of $W = 5$ with a P_{fa} of 10^{-4} the P_d assumes value of 0.1386 for detector (6) while it is 0.2822 for detector (10) and 0.9913 for the detector (12). Moreover it is worthwhile to note that for all the detectors the P_d improves as W increases for a given P_{fa}. This effect is principally due to the more accurate estimation of the covariance matrices which exploits more homogeneous data.

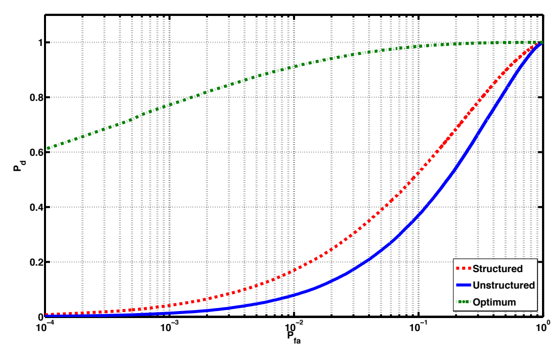

Fig. 2: P_d versus P_{fa} for $W = 3$.

B. Testing on Real Data

In this subsection the performance analysis on real X-band data is presented. The dataset used is the Coherent Change Detection Challenge dataset acquired by the Air Force Research Laboratory (AFRL) [8], the data contains passes acquired with three polarizations (HH, VV, and HV).

For our analysis we focus on two acquisitions from the entire dataset, unfortunately the ground truths of the data is not available (e.g. the actual changes between two different acquisitions), so the selection of two passes providing the opportunity to generate a sufficiently accurate ground truth was required. For this reason the best candidates which is those obtained for two passes: the acquisition named “FP0124”

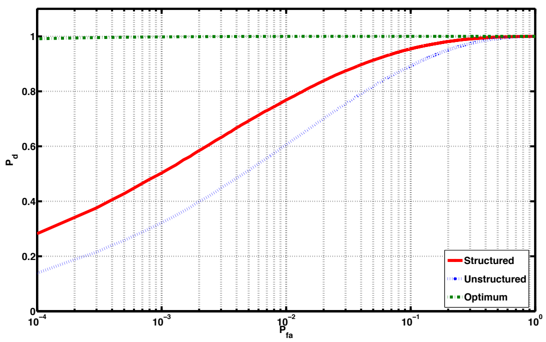

Fig. 3: P_d versus P_{fa} for $W = 5$.

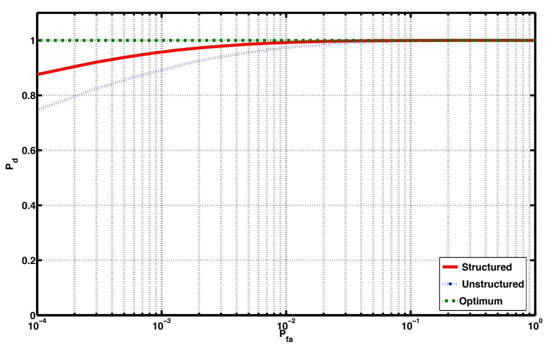

Fig. 4: P_d versus P_{fa} for $W = 7$.

is used as reference pass, while the acquisition “FP0121”, is used as a test pass. The selected area of interest is a sub-image of 1000×1000 pixels (i.e., $L = M = 1000$) and is composed of several parking lots which are occupied by numerous parked, (i.e., stationary) vehicles. For this particular scenario the changes between the reference and test images (denoted by $\boldsymbol{X}$ and $\boldsymbol{Y}$ respectively), occurred during the time interval between the two acquisitions, and can be distinguished in the following two cases:

- a vehicle is present in $\boldsymbol{X}$ but is not present in $\boldsymbol{Y}$, this case is referred as departure;
- a vehicle is not present in $\boldsymbol{X}$ but is present in $\boldsymbol{Y}$, this event is referred as arrival.

Using the cases defined above, a total of 34 changes between $\boldsymbol{X}$ and $\boldsymbol{Y}$ can be visually identified (by flickering the two images). The resulting ground truth is shown in Figure 5-a, wherein the black rectangle represent departures and the white rectangles indicate arrivals.

Although the acquisitions were performed during the same day and the images were registered, the returns from a scatterer can contribute differently to neighbour pixels, for example a slightly different aspect angle can produce a different amount of energy spill-over. These relative differences in the imaged data can lead to false alarms in the change detection results. For this reason we consider a guard area around each arrival-departure. This allows the definition of an extended ground truth (see Figure 5-b) used in the following to compare the performance of the considered detection algorithms.

In order to assess the performance of the detectors both the

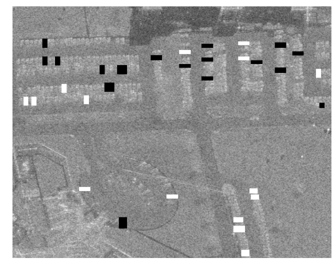

(a) Ground truth.

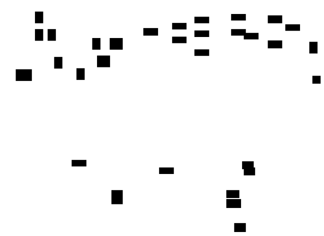

(b) Ground truth with guard cells.

Fig. 5: Ground truth superimposed to the reference image and ground truth with the addition of guard cells.

number of detected changes and the change detection maps are presented. For the i-th receiver, the corresponding map of changes $\boldsymbol{C}_i$, is a $L \times M$ matrix whose (l, m)-th entry is the i-th decision statistic considering the $N \times N$ sample Grammian matrix $\boldsymbol{S}_{X_{l,m}}$ ($\boldsymbol{S}_{Y_{l,m}}$) evaluated considering a square neighbourhood[1] with size $W \times W$ of the pixel (l, m) of $\boldsymbol{X}$ ($\boldsymbol{Y}$).

The detection map corresponding to $\boldsymbol{C}_i$, is then defined as

$$\boldsymbol{D}_i(l,m) = \begin{cases} 1 & \text{if } \boldsymbol{C}_i(l,m) > T_i \qquad l = 1, \ldots, L \\ 0 & \text{otherwise} \qquad\quad m = 1, \ldots, M \,. \end{cases} \tag{13}$$

where T_i denotes the detection threshold. In the analysis presented in this section, the thresholds are set to ensure $P_{fa} = 10^{-3}$ in the complement of the extended ground truth area, namely, in the region where no changes occur (there are no true positives). This means that, for each detector, after computing the decision statistics (for each pixel belonging to the complement of the extended ground truth), the threshold has been selected in order that

$$10^{-3} \times \text{total number of available statistics (trials)}\,,$$

[1]We notice that, in order to obtain $\boldsymbol{C}_i$ of size $L \times M$ we include a frame of ε pixels width of both reference and test images with $\varepsilon = \frac{W-1}{2}$, in order to be able to compute the statistics on the image borders. By doing so, W must be odd.

are greater than the threshold. This ensures that all the comparisons refer to the same P_{fa} level, namely the number of threshold crossings in the complement of the extended ground truth is exactly the same for all the analysed detectors. In Table I the number of correct changes detected using receivers (6) and (10) for the cases with $W = 3$, $W = 5$, and $W = 7$ are reported.

	W		
Detector	3	5	7
Unstructured GLRT (6)	3802	6492	7533
Structured GLRT (10)	4949	6655	7387

TABLE I: Number of correct detections for $W = 3$, 5 and 7.

From Table I it is clear that the structured GLRT outperforms the unstructured GLRT for the smaller window sizes ($W = 3$ and 5) whereas the unstructured GLRT outperforms the structured GLRT for the larger window size of $W = 7$ when it is able to detect more changes in the image. This last result can be justified in terms of a covariance model mismatch in the sense that the off-diagonal entries of the polarimetric covariance matrix which in the theoretical model have been set to zero might not be exactly zero in reality (even if very close to that value). Additionally there might be some other deviations from the theoretical model for instance due to environmental non-homogeneities.
Last results presented are example of detection maps for detectors (6) and (10) for the case of $W = 3$ in Figure 6-a and in Figure 6-b respectively. From the detection maps the higher number of detection achievable with the detector (10) is appreciable.

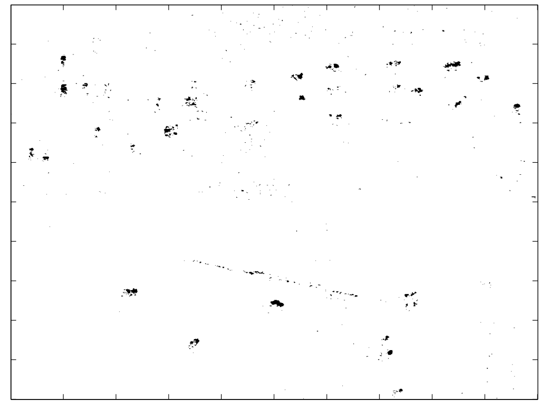

(a) Detector (6).

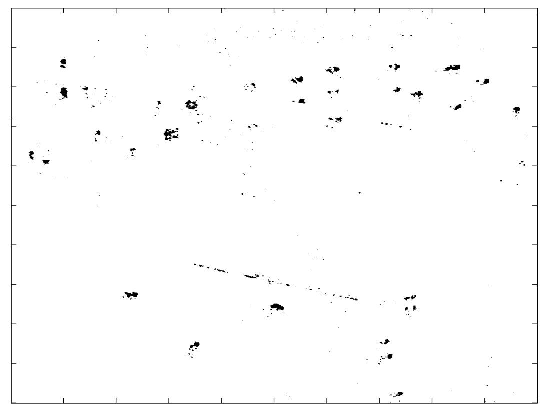

(b) Detector (10).

Fig. 6: Detection maps for $W = 3$.

V. Conclusions

The block-diagonal structure for the polarimetric covariance matrix is exploited in this paper to derive a new decision rule based on the GLRT criterion. The proposed approach ensures the CFAR property with respect to the unknown polarimetric covariance. The novel structured GLRT detector has been compared with the unstructured GLRT, with analysis on both simulated and real full-polarimetric SAR data. The performance analysis confirmed that a structured approach can provide increased performance with particular benefits when a small amount of homogeneous data is available. Future work will concentrate on the performance analysis on other datasets, the study of model sensitivity mismatches, and the development of an invariant framework accounting at the maximal invariant design stage of the block-diagonal structure of the polarimetric covariance matrix.

Acknowledgment

This work was supported by the Engineering and Physical Sciences Research Council (EPSRC) Grant number EP/K014307/1 and the MOD University Defence Research Collaboration in Signal Processing and the University of Naples "Federico II".

References

[1] M. Preiss and N. J. S. Stacy, "Coherent Change Detection: Theoretical Description and Experimental Results", Intelligence, Surveillance and Reconnaissance Division, Defence Science and Technology Organisation, DSTO-TR-1851.

[2] R. Touzi, A. Lopes, J. Bruniquel, and P. W. Vachon, "Coherence Estimation for SAR Imagery", IEEE Trans. on Geosci. Remote Sens., vol. 37, no. 1, pp. 135-149, Jan. 1999.

[3] L. M. Novak, "Change Detection for Multi-polarization, Multi-pass SAR", SPIE Conference on Algorithms for Synthetic Aperture Radar Imagery XII, Orlando, FL, pp. 234-246, March 2005.

[4] K. Conradsen, A. A. Nielsen, J. Schou, and H. Skriver, "A Test Statistic in the Complex Wishart Distribution and Its Application to Change Detection in Polarimetric SAR Data", IEEE Trans. on Geosci. Remote Sens., vol. 41, no. 1, pp. 4-19, Jan. 2003.

[5] V. Carotenuto, A. De Maio, C. Clemente, and J. J. Soraghan, "Multi-Polarization SAR Change Detection with Invariant Decision Rules", Submitted to IEEE RadarCon 2014, Cincinnati.

[6] L. M. Novak and M.C. Burl, "Optimal speckle reduction in polarimetric SAR imagery", IEEE Trans. on Aerospace and Electronic Systems, vol.26, no.2, pp.293-305, March 1990.

[7] H. L. Van Trees, *Detection, Estimation, and Modulation Theory*, Pt. 1, John Wiley & Sons, 1968.

[8] S. Scarborough, L. Gorham, M. J. Minardi, U. K. Majumdar, M. G. Judge, L. Moore, L. Novak, S. Jaroszewski, L. Spoldi, and A. Pieramico, "A Challenge Problem for SAR Change Detection and Data Compression", Proc. SPIE 7699, Algorithms for Synthetic Aperture Radar Imagery XVII, 76990U, doi:10.1117/12.855378, Apr. 18, 2010.